Japanese Journal of Applied Physics **55**, 036504 (2016)
http://doi.org/10.7567/JJAP.55.036504

REGULAR PAPER

Effect of carbon situating at end-of-range defects on silicon self-diffusion investigated using pre-amorphized isotope multilayers

Taiga Isoda, Masashi Uematsu, and Kohei M. Itoh*

School of Fundamental Science and Technology, Keio University, Yokohama 223-8522, Japan

*E-mail: kitoh@appi.keio.ac.jp

Received October 10, 2015; revised November 23, 2015; accepted December 19, 2015; published online February 22, 2016

The effect of implanted carbon (C) on silicon (Si) self-diffusion has been investigated using pre-amorphized $^{28}Si/^{nat}Si$ multilayers. The isotope multilayers were pre-amorphized by Ge implantation followed by C implantation, and annealed at 950 °C. Because of the presence of C, the Si self-diffusion was slower in 30 min annealing than the self-diffusion without C. This was attributed to the trapping of Si self-interstitials by C. On the other hand, the Si self-diffusion with C was faster in 2 h annealing than the self-diffusion without C, except in the end-of-range (EOR) defect region. The cause of this enhanced diffusion was understood as the retardation of Ostwald ripening of EOR defects by C trapped at the defects. In the EOR defect region, however, Si self-diffusion was slower than the self-diffusion without C in both 30 min and 2 h annealing owing to the presence of C. Relaxation of the tensile strain associated with the EOR defects by the trapped C was proposed to be the main cause of the retarded diffusion in the EOR region.

1. Introduction

Codoping of carbon (C) in silicon (Si)[1–13] is one of the most important methods for the formation of ultrashallow junctions because C reduces transient-enhanced diffusion (TED) by trapping Si self-interstitials (I's) generated by ion implantation. The mechanism of reducing TED has been studied by codoping C with boron (B) during crystal growth by molecular beam epitaxy (MBE), using B atoms as markers.[11,12] The reduction mechanism is described by[11,13]

$$C_s + C_s + I \leftrightarrow C_s + C_i \leftrightarrow C_sC_i, \quad (1)$$

where C_s and C_i denote C in substitutional and interstitial sites, respectively. This reaction (1) means that two C atoms and one I form an immobile C_sC_i cluster. As a method of introducing C, in addition to C codoping during crystal growth, C co-implantation, which is often used in Si device processing because of its compatibility with conventional device processing, has been investigated.[1–10]

In our previous study,[4] Si self-, B and C diffusions were simultaneously observed using isotopically enriched ^{28}Si and natural Si (^{nat}Si) multilayers that were co-implanted with B and C, where the doses were too low to amorphize the sample but high enough to form immobile BI clusters.[14,15] The results showed that B diffusion near the kink region was reduced owing to the slower dissolution of immobile BI clusters with higher C dose. On the other hand, Si self-diffusion was enhanced with higher C dose. These results indicate that the reduction of B diffusion is not due to the I trapping by the formation of C_sC_i clusters, but due to the retardation of BI cluster dissolution by the presence of C, thereby decreasing the amount of mobile B. Moreover, the formation of CI clusters[3,13] with excess I's induced by ion implantation prevents the formation of C_sC_i clusters. In contrast, the excess I's induced by ion implantation can be eliminated by pre-amorphizing implants (PAIs) because solid-phase epitaxial (SPE) regrowth of the amorphous region almost totally eliminates the damage in the regrown region.[8,16] Therefore, the formation of CI clusters would be prevented by SPE regrowth by C implantation in pre-amorphized Si, and C atoms are embedded into the substitutional sites. Then the I trapping by the formation of C_sC_i clusters becomes effective for C implantation in the same way as for C doping during crystal growth. We have observed Si self-diffusion in the presence of end-of-range (EOR) defects using $^{28}Si/^{nat}Si$ multilayers that were amorphized by Ge implantation.[17] EOR defects are interstitial-type dislocation loops formed below the amorphous/crystalline (a/c) interface, and lattice expansion, that is, positive volume change of a Si crystal, due to EOR defects causes tensile strain. The tensile strain induced by EOR defects is estimated to be about 1×10^{-2} from X-ray analysis.[18–20] In addition to the TED induced by EOR defects, we have found further enhancement of Si self-diffusion by the tensile strain associated with EOR defects in the defect region.[17]

Cristiano et al. reported that the presence of C causes retardation of Ostwald ripening of EOR defects.[10] To the best of our knowledge, however, the influence of this retardation on diffusion in Si and on the behavior of I's has not yet been reported. In the present work, we observe Si self-diffusion in pre-amorphized $^{28}Si/^{nat}Si$ multilayers that are implanted with C and Ge. The behavior of I's is directly investigated by examining the ^{30}Si self-diffusion. Using Si isotope multilayers, the effect of C on the behavior of I's is observed without any disturbance by other possibilities such as B trapping by EOR defects[21] and CI clustering. We investigate the effect of the presence of C in pre-amorphized Si on Ostwald ripening of EOR defects and on the enhancement of Si self-diffusion by the tensile strain originating from the EOR defects.

2. Experimental procedure

Isotope multilayers that were composed of the alternating layers of isotopically enriched ^{28}Si and natural Si (^{28}Si: 92.2%, ^{29}Si: 4.7%, ^{30}Si: 3.1%) were grown by solid-source MBE.[22–24] A (100)-oriented B-doped Czochralski Si wafer with a resistivity of 1–20 Ω cm was used as a substrate. A ~150-nm-thick ^{nat}Si buffer layer was grown prior to the growth of the isotope multilayers in order to achieve an atomically smooth surface. The isotope multilayers are composed of nine ^{28}Si layers 28 nm thick separated from each other by a ^{nat}Si layer 17 nm thick. ^{nat}Si layers had the natural abundance, i.e., 3.1%, of ^{30}Si, whereas ^{28}Si layers were depleted of ^{30}Si. The isotope multilayers were first amor-

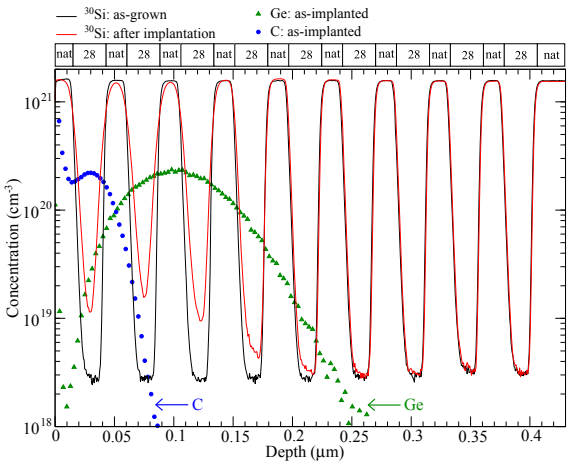

Fig. 1. (Color online) SIMS profiles of ^{30}Si in the ^{nat}Si/^{28}Si isotope multilayers before (as-grown) and after (after implantation) Ge and C implantation. The implanted Ge (150 keV, 2×10^{15} cm^{-2}) and C (10 keV, 1×10^{15} cm^{-2}) depth profiles are also presented. Solid lines represent the profiles of ^{30}Si and symbols those of Ge and C. The structure of isotope multilayers is schematically shown at the top of the figure.

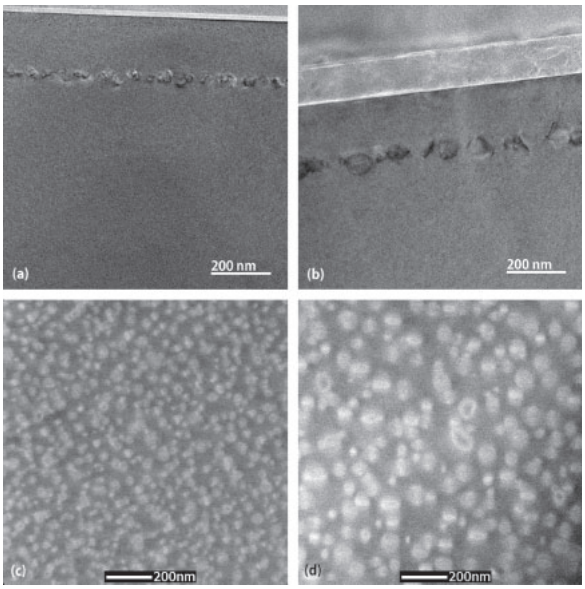

Fig. 2. TEM and STEM images of EOR defects in samples with and without C annealed at 950 °C for 2 h. Bright-field cross-sectional TEM images of samples (a) with and (b) without C. Dark-field plan-view STEM images of samples (c) with and (d) without C.

phized by ^{74}Ge^{+} ion implantation with an energy of 150 keV and a dose of 2×10^{15} cm^{-2} at room temperature. After the pre-amorphization, ^{12}C^{+} was implanted in the amorphous region with an energy of 10 keV and a dose of 1×10^{15} cm^{-2} at room temperature. The dose of C implantation was selected such that the C concentration resembles that in actual device structures.[25] Pre-amorphized Si isotope multilayers without C implantation were also prepared as a control sample.

The isotope multilayers were annealed at 950 °C in a resistance furnace under an Ar (99.99%) atmosphere. The annealing temperature of 950 °C was chosen in this study because the effect of EOR defects on Si self-diffusion was clearly observed at this temperature in our recent study.[17] The observations by cross-sectional transmission electron microscopy (TEM) and plan-view scanning transmission electron microscopy (STEM) were performed with an acceleration voltage of 200 keV. Si self-diffusion was evaluated by observing the change in the ^{30}Si depth profiles after annealing. The depth profiles of ^{30}Si, ^{12}C, and ^{74}Ge were measured by secondary ion mass spectrometry (SIMS). The primary ions used in SIMS were O^{2+} with an energy of 1.0 keV for ^{30}Si, and Cs^{+} with 3.0 keV for ^{12}C and ^{74}Ge.

3. Results

Figure 1 shows the depth profile of ^{30}Si in the Si isotope multilayers before the implantation of Ge and C (as-grown) measured by SIMS. The ^{nat}Si/^{28}Si periodic structure is schematically shown at the top of the figure. The actual interfaces between the ^{nat}Si and ^{28}Si layers are abrupt (the degree of intermixing is only two atomic layers)[22–24] and the smearing of the ^{nat}Si and ^{28}Si profiles is due to SIMS artifacts (knock-on mixing, etc.). The periodic profile was perturbed after the implantation of Ge and C (after implantation), as shown in Fig. 1, where the depth profiles of Ge and C are also presented. This perturbation of the profile is due to Si displacement induced by Ge implantation.[26] Because of the implantation, amorphization occurred between the surface and 175 nm in depth, while the deeper region ($x > 175$ nm) remained single crystalline, as was shown in Fig. 2(a) of our previous study for the same implantation conditions.[17] Figures 2(a) and 2(b) show the cross-sectional TEM images of the samples annealed for 2 h with and without C implantation, respectively. EOR defects are formed just beneath the former a/c interface, i.e., at the depth of 175–225 nm, as was observed in our previous study.[17] No significant difference in the position of EOR defects was observed between the samples with and without C implantation. Figures 2(c) and 2(d) show the plan-view STEM images of the samples with and without C implantation annealed for 2 h, respectively. The histograms of the loop radius distribution of EOR defects [Figs. 3(a) and 3(b)] were obtained by counting the loops seen in the contrast of plan-view STEM images in Figs. 2(c) and 2(d). The result shows that the mean radius of the loops tends to become smaller owing to the presence of C. This tendency is consistent with the result, obtained by Cristiano et al.,[10] that Ostwald ripening of EOR defects is retarded by the presence of C.

Figure 4 shows the depth profiles of C in the samples with C implantation annealed at 950 °C for 30 s, 30 min, and 2 h. The C profiles exhibit a peak at a depth of ~200 nm, which indicates C trapping at EOR defects, and the C concentration of the peak increases with annealing time. In contrast, the C concentration at the implanted peak (~40 nm) first decreases during the 30 min annealing but remains almost unchanged after the 30 min annealing. Figures 5(a) and 5(b) show the depth profiles of ^{30}Si in the samples with C implantation annealed at 950 °C for 30 s, 30 min, and 2 h. At the fifth ^{28}Si layer of the isotope multilayers, whose region coincides with the position of EOR defects, the ^{30}Si profiles show faster Si self-diffusion than in the other layers because of the tensile strain associated with the EOR defects [see Fig. 5(b)], as has been reported in Ref. 17. Figures 6(a) and 6(b) show the ^{30}Si profiles with and without C implantation after annealing for 30 min and 2 h. The profiles for 30 s with and without C are not shown in this figure because the amount of diffusion during the 30 s is so small for both samples that no significant

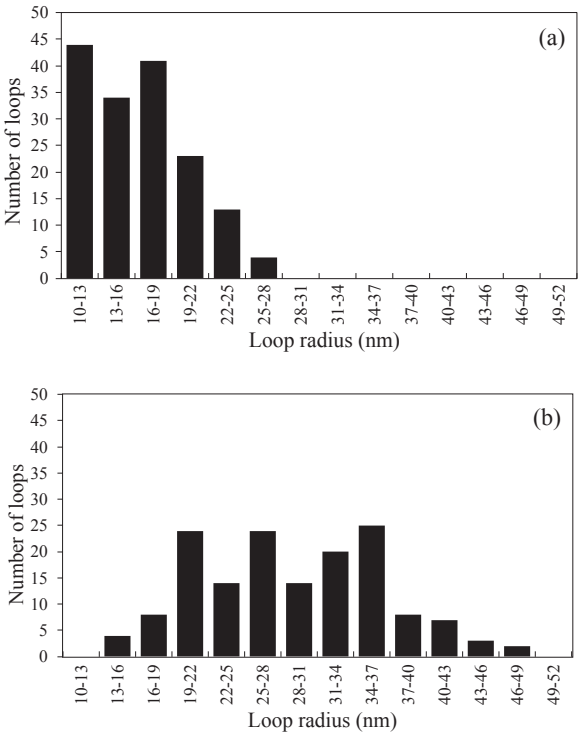

Fig. 3. Histograms of the loop radius distribution of EOR defects (a) with and (b) without C obtained by counting the loops revealed by the contrast of plan-view STEM images.

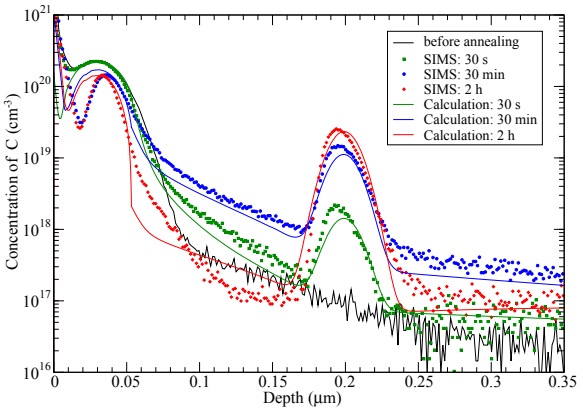

Fig. 4. (Color online) SIMS and calculated profiles of C with 150 keV, 2×10^{15} cm^{-2} Ge and 10 keV, 1×10^{15} cm^{-2} C implantations, and annealing at 950 °C for 30 s, 30 min, and 2 h. Symbols and solid lines represent SIMS and calculated profiles, respectively. The SIMS profile before annealing is also shown by the thick solid line.

difference is seen between the two profiles. Figure 7 shows the ratio of the time-averaged self-diffusivity with C to that without C at the positions of each valley in the ^{30}Si profile of the isotope multilayers. The time-averaged Si self-diffusivities were derived from each ^{30}Si profile with and without C in Fig. 6(a). A ratio smaller than unity means the retardation of Si self-diffusion by the presence of C with respect to that without C, while a ratio larger than unity means the enhancement. For 30 min annealing, Si self-diffusion is retarded by 30–40% in the region shallower than EOR defects and by about 10% in the deeper region owing to the presence of C. This retardation is attributed to I trapping by the formation of C_sC_i clusters[11,13] and is in accordance with expectations based on C implantation in pre-

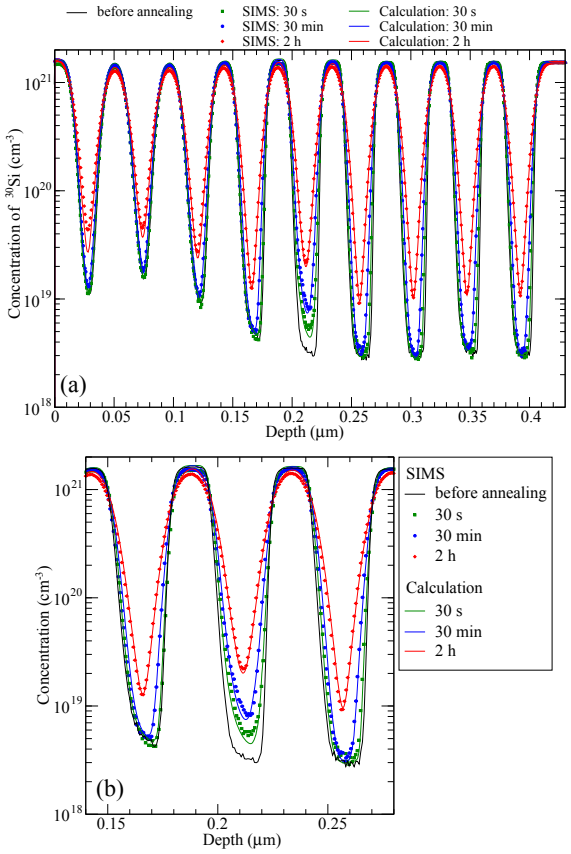

Fig. 5. (Color online) SIMS and calculated profiles of ^{30}Si with 150 keV, 2×10^{15} cm^{-2} Ge and 10 keV, 1×10^{15} cm^{-2} C implantations, and annealing at 950 °C for 30 s, 30 min, and 2 h. (b) The EOR defect region is enlarged. Symbols and solid lines represent SIMS and calculated profiles, respectively. The SIMS profile before annealing is also shown by a thick solid line.

amorphized Si, where the formation of CI clusters will be prevented by SPE regrowth and C atoms are embedded into the substitutional sites. For 2 h annealing, in contrast, Si self-diffusion is enhanced by the presence of C, except at the fifth ^{28}Si layer of multilayers. At the fifth ^{28}Si layer, whose region coincides with the position of EOR defects, Si self-diffusion is retarded for the cases of both 30 min and 2 h annealing by the presence of C.

4. Discussion

EOR defects grow in size and reduce their density while the total number of Si self-interstitials stored in the loops remains constant upon annealing. This coarsening process, Ostwald ripening, reduces the efficiency of the defects as a source of I's that govern TED.[27] Our TEM results showed that the mean radius of the loops in samples with C is smaller than that in samples without C. This indicates that Ostwald ripening of EOR defects is retarded so that the I concentration is higher than that in the case without C. Therefore, Si self-diffusion is faster than that without C although C can reduce TED by trapping I's. This fast diffusion is more likely to be observed for longer annealing because the duration of Ostwald ripening of EOR defects is usually longer than that of the formation of C_sC_i clusters. As shown in Fig. 7, Si self-diffusion is retarded in 30 min annealing while it is enhanced in 2 h annealing by the presence of C. In the case of 30 min annealing, the slowing down of self-diffusion owing to I trapping by the formation of C_sC_i clusters[11,13] is more

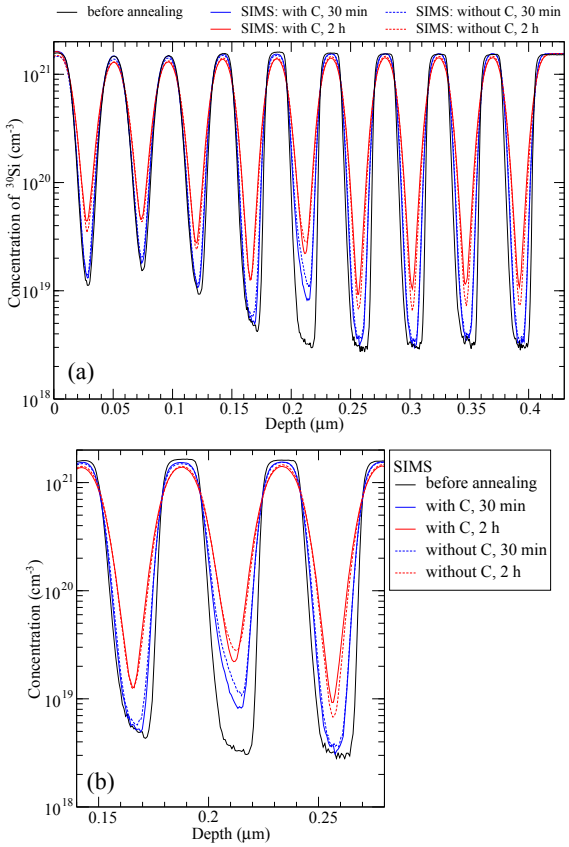

Fig. 6. (Color online) Self-diffusion in pre-amorphized Si with C and without C. (a) SIMS profiles of ^{30}Si in pre-amorphized Si with and without C implantation (10 keV, 1×10^{15} cm^{-2}) and annealed at 950 °C for 30 min and 2 h. (b) The EOR defect region is enlarged. Solid and dashed lines represent the SIMS profiles of the samples with and without C implantation, respectively. The SIMS profile before annealing is also shown by a thick solid line.

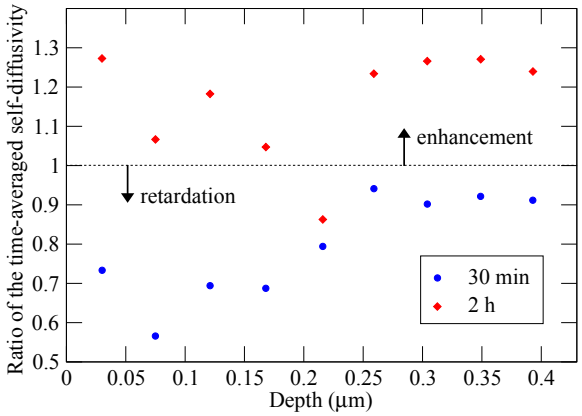

Fig. 7. (Color online) Ratio of the time-averaged self-diffusivity with C to that without C as a function of depth. Closed circles and diamonds represent the ratios for 30 min and 2 h annealing, respectively.

dominant than the speeding up of self-diffusion by the retardation of Ostwald ripening. On the other hand, for 2 h annealing, the fast diffusion occurs, where the effect of Ostwald ripening of EOR defects becomes more dominant than that of the formation of C_sC_i clusters, because the formation of C_sC_i clusters saturates during long-time annealing.

Si self-diffusion in the EOR defect region is enhanced by the tensile strain associated with EOR defects.[17] In the present study, the Si self-diffusion is retarded in both 30 min and 2 h annealing by the presence of C, as shown in Fig. 7. In 30 s annealing, however, no significant difference is seen between the samples with and without C (not shown in the figure). These results are attributable to the relaxation of the tensile strain by the C trapping at the EOR defects. As shown in Fig. 4, C atoms trapped at EOR defects increase with annealing time, and hence, the tensile strain is reduced with time. Then the diffusion enhancement by the tensile strain is reduced with time. In addition, the diffusion enhancement by the tensile strain (×27 at $t = 0$) is significantly greater than that by the supersaturated I's from EOR defects (× ~3). Therefore, Si self-diffusion in the EOR defect region is retarded in both 30 min and 2 h annealing by the presence of C, but no retardation is observed in 30 s annealing.

Recently, we developed a model where Si self-diffusion is enhanced by the tensile strain associated with EOR defects and that this enhancement is suppressed with increasing mean radius of EOR defects due to Ostwald ripening.[17] Using this model, we shall analyze the ^{30}Si self-diffusion observed in the present study by taking into account the retardation of Ostwald ripening of EOR defects and the relaxation of the tensile strain at EOR defects by the presence of C. The present calculation includes TED by EOR defects and {311} clusters, and the enhancement of Si self-diffusion by the tensile strain associated with EOR defects,[17] and C diffusion and the formation of C_sC_i clusters discussed in Ref. 3. C segregation at the surface is also taken into account to reproduce the significant reduction of C concentration near the surface (Fig. 4). In order to take into account the effect of C at EOR defects on Si self-diffusion, we add C trapping at EOR defects to the diffusion models. C trapping at EOR defects is described by

$$\frac{\partial C_{\mathrm{trap}}}{\partial t} = K_{\mathrm{trap}} C_{\mathrm{i}} - K_{\mathrm{detrap}} C_{\mathrm{trap}}, \tag{2}$$

$$K_{\mathrm{trap}} = k_{\mathrm{trap}} \exp\left[\frac{-(x - A_1)^2}{2A_2^2}\right], \tag{3}$$

where C_{trap} is the concentration of C trapped at EOR defects. Here, K_{trap} and K_{detrap} represent the trapping and detrapping rates, respectively, and k_{trap} is the maximum trapping rate. We assume that k_{trap} has a Gaussian shape with the peak position A_1 and the width A_2. C trapping is taken into account by adding (a) Eq. (2) to the C diffusion equations of Ref. 3 and (b) the right-hand side of Eq. (2) to Eq. (8) of Ref. 3 as the reaction term. C detrapping is not taken into account in the calculation ($K_{\mathrm{detrap}} = 0$) because no decrease in the concentration of C trapped at EOR defects is observed. Besides C trapping at EOR defects, the C profiles at the implanted peak (~40 nm) are practically unchanged after the 30 min annealing. This is attributable to the formation of C precipitation at the C implanted peak. C atoms precipitate when the C concentration exceeds a certain critical value (8×10^{19} cm^{-3} was used in the present calculation), as has been done for a high concentration of As in Si.[28] Using all the models mentioned above, diffusion equations are solved numerically using the partial differential equation solver ZOMBIE.[29] The SIMS profiles are well reproduced when $k_{\mathrm{trap}} = 7 \times 10^6$ s^{-1}, $A_1 = 200$ nm, and $A_2 = 10$ nm.

The solid lines in Figs. 4 and 5 show the calculated profiles of C and ^{30}Si, respectively, after annealing for 30 s, 30 min, and 2 h. The calculation reproduces the SIMS

profiles very well, except for the diffusion in the ^{28}Si layers near the surface for 2 h annealing being underestimated. In the calculation, the coarsening rate of Ostwald ripening K is decreased in order to take into account the retardation of Ostwald ripening of EOR defects. When the K value is reduced to 1/10 of the original value reported by Bonafos et al.,[27] the ^{30}Si profiles for 30 s, 30 min, and 2 h annealing, except in the EOR defect region, are fitted well, and hence, the enhancement of Si self-diffusion owing to the retardation of Ostwald ripening of EOR defects is well reproduced. The fitting using the constant value of reduced K indicates that the reduction of K owing to C saturates at the C concentration of $\sim 10^{18}$ cm^{-3} in the early stage of annealing. Concerning the relaxation of the tensile strain associated with EOR defects owing to the presence of C, the strain enhancement factor at $t = 0$, f_0^{st}, decreased with time. The ^{30}Si profiles can be fitted using $f_0^{st} = 27$ for 30 s annealing, $f_0^{st} = 10$ for 30 min annealing, and $f_0^{st} = 2.5$ for 2 h annealing in the calculation. In our previous study for the sample without C implantation, the enhanced Si self-diffusion owing to the tensile strain associated with EOR defects is well reproduced using the constant value of $f_0^{st} = 27$ for all annealing times.[17] The decreasing f_0^{st} with time indicates that the tensile strain at EOR defects relaxes as more C is trapped at EOR defects. For 30 s annealing, however, the amount of C trapped in the EOR defect region is so small that little relaxation of the tensile strain occurs. The calculation above clarifies that C trapped at EOR defects (i) enhances Si self-diffusion owing to the retardation of Ostwald ripening of EOR defects and (ii) retards Si self-diffusion in the EOR defect region because of the local relaxation of the tensile strain.

As mentioned above, the diffusion of the first and second ^{28}Si layers in 2 h annealing was underestimated [see Fig. 5(a)]. This underestimation is due to our assumption in the calculation that the surface is a perfect sink for I's and the I concentration at the surface is maintained at the thermal equilibrium value. Therefore, the underestimation of the Si self-diffusion suggests that the I near the surface region is supersaturated owing to C implantation. Note that the calculation using this assumption well reproduces the Si self-diffusion without C implantation.[17] A possible origin of the I supersaturation near the surface region is the formation of dislocations by C implantation or the change in the surface condition owing to C, either of which would reduce the efficiency of the sink for I's.

5. Conclusion

The effect of C on Si self-diffusion was investigated using pre-amorphized ^{28}Si/^{nat}Si multilayers that are implanted with C and Ge. After the implantation, the isotope multilayers were annealed at 950 °C. Because of the presence of C, Si self-diffusion was retarded for 30 min annealing, which is attributed to the trapping of Si self-interstitials by C via the formation of C_sC_i clusters. In contrast, the diffusion was enhanced for 2 h annealing, except at the EOR defect region. This enhanced diffusion is explained by the retardation of Ostwald ripening of EOR defects because of C trapped at the defects, which, in turn, slows down the reduction of TED by the ripening. The effect of Ostwald ripening of EOR defects becomes more dominant than that of the formation of C_sC_i clusters because the formation of C_sC_i clusters saturates in long-time annealing. At the EOR defect region, on the other hand, Si self-diffusion was retarded for both 30 min and 2 h annealing by the presence of C. This is attributable to the relaxation of the tensile strain associated with EOR defects by the trapped C, which decreases the diffusion enhancement by tensile strain.

Acknowledgments

The authors thank Makoto Kuroda for carrying out the TEM and STEM measurements. This work was supported in part by Grants-in-Aid for Scientific Research from the Japan Society for the Promotion of Science (No. 24560413), NanoQuine, JSPS Core-to-Core Program, and Cooperative Research Project Program of the RIEC, Tohoku University.

1) S. Nishikawa, A. Tanaka, and T. Yamaji, Appl. Phys. Lett. **60**, 2270 (1992).
2) E. C. Jones and E. Ishida, Mater. Sci. Eng. R **24**, 1 (1998).
3) M. Uematsu, J. Appl. Phys. **111**, 073517 (2012).
4) M. Uematsu, K. Matsubara, and K. M. Itoh, Jpn. J. Appl. Phys. **53**, 071302 (2014).
5) E. Augendre, B. J. Pawlak, S. Kubicek, T. Hoffmann, T. Chiarella, C. Kerner, S. Severi, A. Falepin, J. Ramos, A. De Keersgieter, P. Eyben, D. Vanhaeren, W. Vandervorst, M. Jurczak, P. Absil, and S. Biesemans, Solid-State Electron. **51**, 1432 (2007).
6) C. H. Poon, A. See, Y. L. Tan, M. S. Zhou, and D. Gui, J. Appl. Phys. **103**, 084906 (2008).
7) L. A. Edelman, S. Jin, K. S. Jones, R. G. Elliman, and L. M. Rubin, Appl. Phys. Lett. **93**, 072107 (2008).
8) K. C. Ku, C. F. Nieh, J. Gong, L. P. Huang, Y. M. Sheu, C. C. Wang, C. H. Chen, H. Chang, L. T. Wang, T. L. Lee, S. C. Chen, and M. S. Liang, Appl. Phys. Lett. **89**, 112104 (2006).
9) N. E. B. Cowern, A. Cacciato, J. S. Custer, F. W. Saris, and W. Vandervorst, Appl. Phys. Lett. **68**, 1150 (1996).
10) F. Cristiano, C. Bonafos, A. Nejim, S. Lombardo, M. Omri, D. Alquier, A. Martinez, S. U. Campisano, P. L. F. Hemment, and A. Claverie, Nucl. Instrum. Methods Phys. Res., Sect. B **127–128**, 22 (1997).
11) S. Mirabella, A. Coati, D. De Salvador, E. Napolitani, A. Mattoni, G. Bisognin, M. Berti, A. Carnera, A. V. Drigo, S. Scalese, S. Pulvirenti, A. Terrasi, and F. Priolo, Phys. Rev. B **65**, 045209 (2002).
12) P. A. Stolk, D. J. Eaglesham, H. J. Gossmann, and J. M. Poate, Appl. Phys. Lett. **66**, 1370 (1995).
13) R. Pinacho, P. Castrillo, M. Jaraiz, I. Martin-Bragado, J. Barbolla, H. J. Gossmann, G. H. Gilmer, and J. L. Benton, J. Appl. Phys. **92**, 1582 (2002).
14) T. E. Haynes, D. J. Eaglesham, P. A. Stolk, H. J. Gossmann, D. C. Jacobson, and J. M. Poate, Appl. Phys. Lett. **69**, 1376 (1996).
15) M. Uematsu, J. Appl. Phys. **84**, 4781 (1998).
16) H. S. Chao, S. W. Crowder, P. B. Griffin, and J. D. Plummer, J. Appl. Phys. **79**, 2352 (1996).
17) T. Isoda, M. Uematsu, and K. M. Itoh, J. Appl. Phys. **118**, 115706 (2015).
18) P. Zaumseil, U. Winter, F. Cembali, M. Servidori, and Z. Sourek, Phys. Status Solidi A **100**, 95 (1987).
19) A. Pesek, Appl. Phys. A **58**, 141 (1994).
20) S. Solmi, F. Cembali, R. Fabbri, M. Servidori, and R. Canteri, Appl. Phys. A **48**, 255 (1989).
21) E. M. Bazizi, P. F. Fazzini, C. Zechner, A. Tsibizov, H. Kheyrandish, A. Pakfar, L. Ciampolini, C. Tavernier, and F. Cristiano, Mater. Sci. Eng. B **154–155**, 275 (2008).
22) Y. Shimizu, M. Uematsu, and K. M. Itoh, Phys. Rev. Lett. **98**, 095901 (2007).
23) Y. Shimizu, M. Uematsu, K. M. Itoh, A. Takano, K. Sawano, and Y. Shiraki, J. Appl. Phys. **105**, 013504 (2009).
24) T. Kojima, R. Nebashi, K. M. Itoh, and Y. Shiraki, Appl. Phys. Lett. **83**, 2318 (2003).
25) A. Mineji and S. Shishiguchi, IEEE Int. Workshop Junction Technology, 2006, p. 84.
26) Y. Shimizu, M. Uematsu, K. M. Itoh, A. Takano, K. Sawano, and Y. Shiraki, Appl. Phys. Express **1**, 021401 (2008).
27) C. Bonafos, D. Mathiot, and A. Claverie, J. Appl. Phys. **83**, 3008 (1998).
28) M. Uematsu, Jpn. J. Appl. Phys. **39**, 1006 (2000).
29) W. Jüngling, P. Pichler, S. Selberherr, E. Guerrero, and H. W. Pötzl, IEEE Trans. Electron Devices **32**, 156 (1985).